Journal of Solid State Chemistry **145,** 260–266 (1999)
Article ID jssc.1999.8261, available online at http://www.idealibrary.com on IDEAL®

Synthesis, Crystal Chemistry, and Electrical Properties of the Intergrowth Oxides $Sr_{4-x}Ca_xFe_{6-y}Co_yO_{13+\delta}$

S. Guggilla, T. Armstrong, and A. Manthiram[1]

Texas Materials Institute, ETC 9.104, The University of Texas at Austin, Austin, Texas 78712

Received October 9, 1998; in revised form February 19, 1999; accepted February 22, 1999

$Sr_{4-x}Ca_xFe_{6-y}Co_yO_{13+\delta}$ oxides crystallizing in an orthorhombic intergrowth structure in which perovskite-type SrO–(Fe, Co)O_2–SrO layers alternate with (Fe, Co)$_2O_{2.5}$ layers along the *b* axis have been synthesized. The Ca solubility decreases from $x = 3.2$ at $y = 0$ to $x = 1.6$ at $y = 1.8$. The cell parameters and volume decrease monotonically with increasing Ca Content. While the unsubstituted $Sr_4Fe_6O_{13+\delta}$ has $\delta \approx 0.4$ excess oxygen, the substitution of Ca and Co tends to decrease the oxygen content and average oxidation state toward, respectively, 13.0 and 3.0+. The total conductivity of $Sr_{4-x}Ca_xFe_{6-y}Co_yO_{13+\delta}$ ($0 \le y \le 0.6$) increases with increasing Ca content *x*, which is in contrast to that found in the perovskite system $Sr_{1-x}Ca_xFeO_{3-\delta}$. The conductivity versus temperature plots of $Sr_{4-x}Ca_xFe_6O_{13+\delta}$ exhibit a change in the sign of the slope from positive to negative at around 450°C for $x \ge 1.6$. While a similar transition in the perovskite system $SrFeO_{3-\delta}$ is related to oxygen loss, no oxygen loss is observed up to at least 900°C in $Sr_{4-x}Ca_xFe_6O_{13+\delta}$. High-temperature X-ray diffraction does not reveal any structural changes up to 750°C and high values of thermoelectric power rule out the possibility of metallic behavior at $T > 450$°C. The observed transition is attributed to a possible redistribution of the charge carriers between the perovskite and nonperovskite layers at $T > 450$°C. © 1999 Academic Press

1. INTRODUCTION

Transition metal oxides with perovskite-related structures have drawn much attention in recent years with respect to, for example, high-temperature superconductivity (1), colossal magnetoresistance (2), oxide-ion conduction (3), and mixed ionic–electronic conduction (4). The mixed ionic–electronic conductors exhibiting both oxide-ion and electronic conductivities have several technological applications. For example, they are of interest as electrodes in solid oxide fuel cells, oxygen separation membranes, sensors, and catalysts. $ABO_{3-\delta}$ (A = alkaline earth and lanthanide, and B = Fe, Co, and Ni) oxides with the three-dimensional perovskite structure are the most widely investigated mixed conductors (4–9). However, the $ABO_{3-\delta}$ perovskite oxides tend to lose oxygen at higher temperatures or under reducing conditions, which often leads to structural transitions, volume changes, and fracture during operation. In addition, the $ABO_{3-\delta}$ perovskites generally have a high electronic component and a much lower ionic component, despite a high total conductivity. These difficulties have limited the use of mixed conductors in some electrochemical devices.

Recently, the composition $SrFeCo_{0.5}O_z$ was reported by Ma *et al.* (10–12) to exhibit mixed conduction with remarkably high oxide-ion conductivity. It was reported to have electronic and ionic conductivities of, respectively, 10 and 7 S cm^{-1} at 800°C and an oxygen flux rate of approximately 7×10^{-6} mol cm^{-2} s^{-1} at 900°C for a membrane 0.75 mm in thickness (12). But Ma *et al.* (10–12) provided no crystal chemical characterization and we showed recently that the composition $SrFeCo_{0.5}O_z$ consists of three phases (13): a predominant perovskite-related intergrowth phase $Sr_4Fe_{6-y}Co_yO_{13}$ ($y \approx 1.5$) that is isostructural with $Sr_4Fe_6O_{13}$ (14, 15), a perovskite phase $SrFe_{1-y}Co_yO_{3-\delta}$, and (3) a face-centered cubic phase (Fe, Co)O_z. The presence of three phases has also been confirmed by Kim *et al.* (16) from electron microprobe analysis. In addition, we have found (17) that the oxygen flux values are three orders of magnitude lower than those reported by Ma *et al.* (12) and our flux values are in close agreement with those found by Kim *et al.* (16).

$Sr_4Fe_6O_{13}$ has an intergrowth structure (Fig. 1) in which perovskite-type SrO–FeO_2–SrO blocks are sandwiched by $Fe_2O_{2.5}$ blocks along the *b*-axis (14). While the Fe atoms in the perovskite layer have a distorted octahedral coordination with the FeO_6 octahedra sharing corners, those in the $Fe_2O_{2.5}$ layers have both distorted tetragonal pyramidal and trigonal bipyramidal oxygen coordinations. The FeO_5 trigonal bipyramids share edges among themselves. Similarly, the FeO_5 tetragonal pyramids share edges among

[1]To whom correspondence should be addressed.

0022-4596/99 $30.00
Copyright © 1999 by Academic Press
All rights of reproduction in any form reserved.

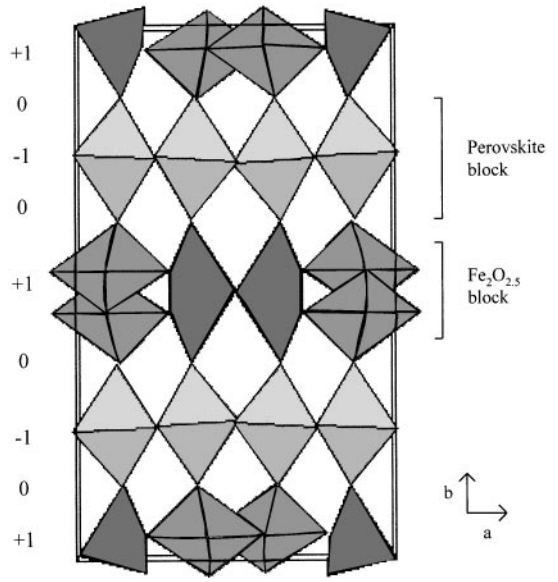

FIG. 1. Crystal structure of $Sr_4Fe_6O_{13}$. The numbers refer to the charges in each layer along the *b*-axis.

themselves. The three types of polyhedra are connected to each other by sharing corners.

We have investigated various cationic substitutions in both the Sr and Fe sites of $Sr_4Fe_6O_{13}$. While attempts to substitute Ba^{2+} for Sr^{2+} result in the formation of the impurity phase $BaSrFe_4O_8$, and to substitute La^{3+} for Sr^{2+} result in the formation of a three-dimensional perovskite phase and $SrFe_{12}O_{19}$, an appreciable amount of Ca^{2+} could be substituted for Sr^{2+}. Although an appreciable amount of Co ($y \approx 1.5$) could be substituted for Fe in $Sr_4Fe_{6-y}Co_yO_{13}$ (13), attempts to substitute Cr, Mn, Ni, Cu, Al, and Ga for Fe result in the formation of a three-dimensional perovskite phase along with $SrFe_{12}O_{19}$ and binary oxide impurities. In this paper, we report the synthesis, crystal chemical characterization, and electrical properties of $Sr_{4-x}Ca_xFe_{6-y}Co_yO_{13}$.

2. EXPERIMENTAL

$Sr_{4-x}Ca_xFe_{6-y}Co_yO_{13}$ samples were synthesized by grinding required amounts of $SrCO_3$, $CaCO_3$, Fe_2O_3, and Co_3O_4 and firing at elevated temperatures. The reaction mixture was first fired at 1100°C for 18 h, then ground, pelletized, and refired at 1150°C for another 18 h. After the firing schedule, the samples were allowed to cool in air in the furnace at a rate of 5°C/min. The products formed were characterized by X-ray powder diffraction and lattice parameters were determined using NaCl as an internal standard. Oxygen content and oxidation state were determined by iodometric titration (18).

Thermogravimetric analysis (TGA) was carried out with a Perkin–Elmer Series 7 Thermal Analysis system. Total conductivity measurements were carried out in air using a four-probe technique with the Van der Pauw configuration.

3. RESULTS AND DISCUSSION

X-ray diffraction data show that single phase $Sr_{4-x}Ca_xFe_6O_{13}$ having the $Sr_4Fe_6O_{13}$intergrowth structure could be obtained for $0 \leq x \leq 3.2$. For $x > 3.2$, the impurity phase $CaFe_2O_4$ is formed. However, the solubility limit of Ca decreases on partly substituting Fe by Co. Figure 2 gives the variation of Ca solubility with Co content in $Sr_{4-x}Ca_xFe_6O_{13}$. Figures 3 and 4 show the variations of the orthorhombic lattice parameters and cell volume with Ca content for $Sr_{4-x}Ca_xFe_6O_{13}$ and $Sr_{4-x}Ca_xFe_{4.5}Co_{1.5}O_{13}$ (25 atom% Co), respectively. The lattice parameters and the cell volume decrease with increasing Ca content due to the substitution of a smaller Ca^{2+} for Sr^{2+}.

Figures 5 and 6 show the variations of, respectively, oxygen content and average oxidation state of Fe and Co with Ca content in $Sr_{4-x}Ca_xFe_{6-y}Co_yO_{13+\delta}$. The unsubstituted $Sr_4Fe_6O_{13+\delta}$ has $\delta \approx 0.4$ excess oxygen. We believe the excess oxygen atoms are accommodated in the $Fe_2O_{2.5}$ layers with a change in the coordination number of Fe from 5 to 6 (13). The substitution of a significant amount of Ca^{2+} for Sr^{2+} in $Sr_{4-x}Ca_xFe_6O_{13+\delta}$ tends to cause a decrease in the excess oxygen and the average oxidation state of Fe. The decrease in oxygen content and oxidation state with Ca content is similar to that found in the perovskite system $Sr_{1-x}Ca_xFeO_{3-\delta}$. The oxygen content and oxidation state also decrease with increasing Co content (13). As a result, for a given Ca content, the oxygen content and oxidation state

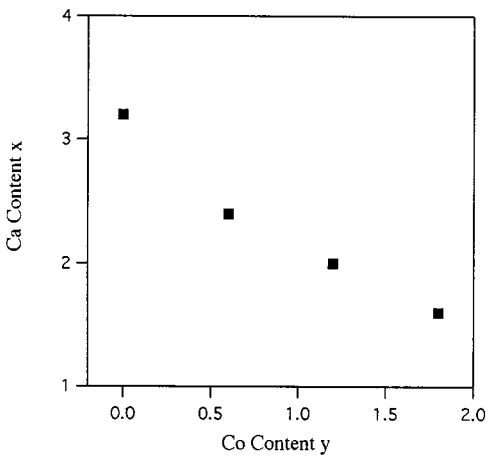

FIG. 2. Variation of the solubility limit of Ca with Co content in $Sr_{4-x}Ca_xFe_{6-y}Co_yO_{13+\delta}$.

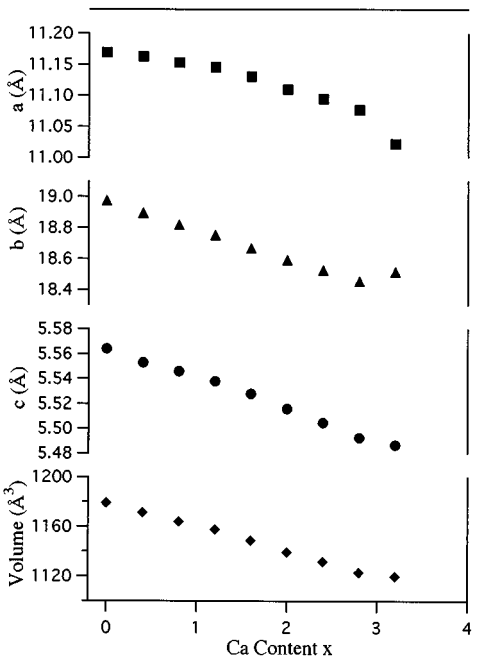

FIG. 3. Variations of lattice parameters and cell volume with Ca content in $Sr_{4-x}Ca_xFe_6O_{13+\delta}$.

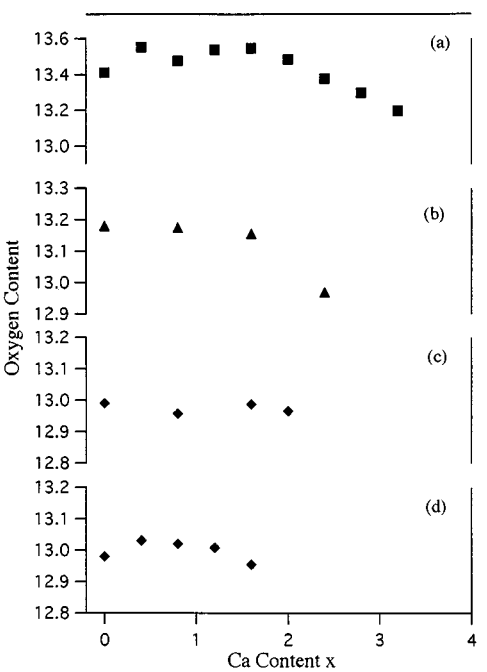

FIG. 5. Variation of oxygen content with Ca content in $Sr_{4-x}Ca_xFe_{6-y}Co_yO_{13+\delta}$: (a) $y = 0$, (b) $y = 0.6$, (c) $y = 1.2$, and (d) $y = 1.5$.

in Figs. 5 and 6 decrease with increasing Co content. The samples with significant amounts of Ca and Co become stoichiometric with respect to oxygen content (13.0) with average oxidation states of 3.0 + for Fe and Co.

Figures 7, 8, and 9 show the variations of total conductivity with temperature for $Sr_{4-x}Ca_xFe_6O_{13+\delta}$ (0 atom% Co), $Sr_{4-x}Ca_xFe_{5.4}Co_{0.6}O_{13+\delta}$ (10 atom% Co), and $Sr_{4-x}Ca_xFe_{4.5}Co_{1.5}O_{13+\delta}$ (25 atom% Co), respectively.

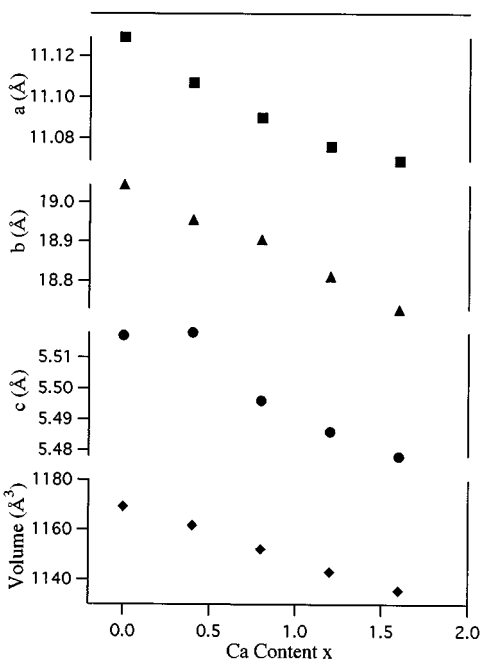

FIG. 4. Variations of lattice parameters and cell volume with Ca content in $Sr_{4-x}Ca_xFe_{4.5}Co_{1.5}O_{13+\delta}$.

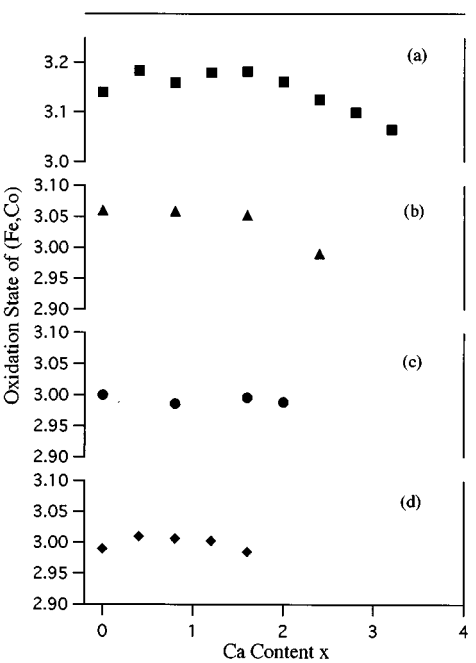

FIG. 6. Variation of average oxidation state of Fe and Co with Ca content in $Sr_{4-x}Ca_xFe_{6-y}Co_yO_{13+\delta}$: (a) $y = 0$, (b) $y = 0.6$, (c) $y = 1.2$, and (d) $y = 1.5$.

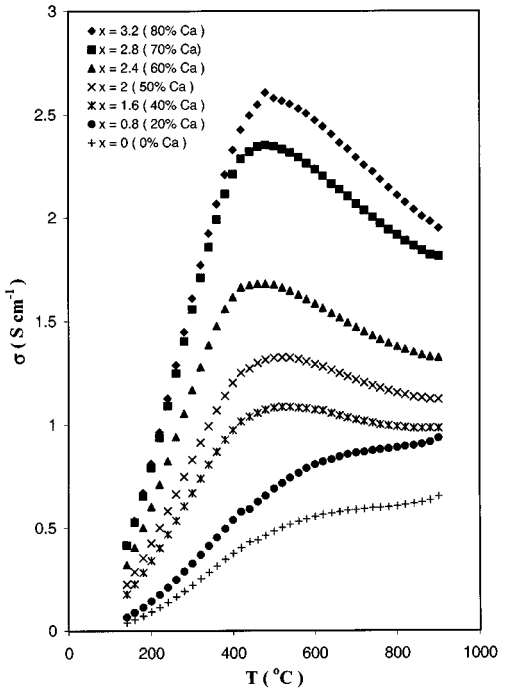

FIG. 7. Variations of total conductivity of $Sr_{4-x}Ca_xFe_6O_{13+\delta}$ with temperature.

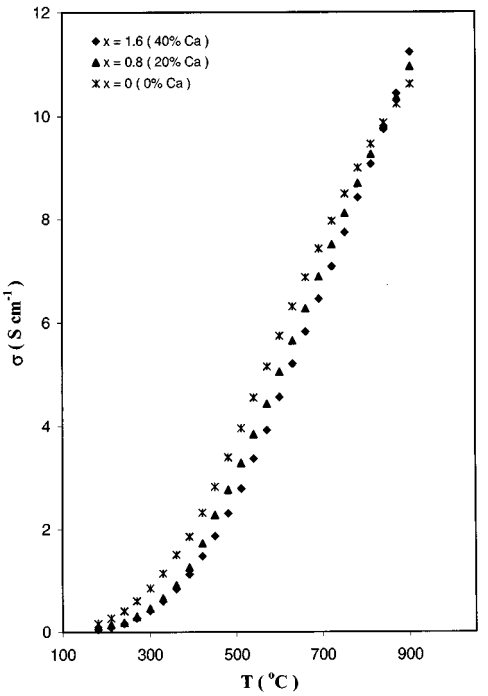

FIG. 9. Variations of total conductivity of $Sr_{4-x}Ca_xFe_{4.5}Co_{1.5}O_{13+\delta}$ (25 atom% Co) with temperature.

Several interesting observations can be made from the conductivity data:

(1) At a given temperature, the conductivity increases with increasing Ca content (Figs. 7 and 8) for samples with low Co content ($0 \le y \le 0.6$). This observation is in contrast to that found in the perovskite system $Sr_{1-x}Ca_xFeO_{3-\delta}$, in which the conductivity decrease with increasing Ca content (Fig. 10).

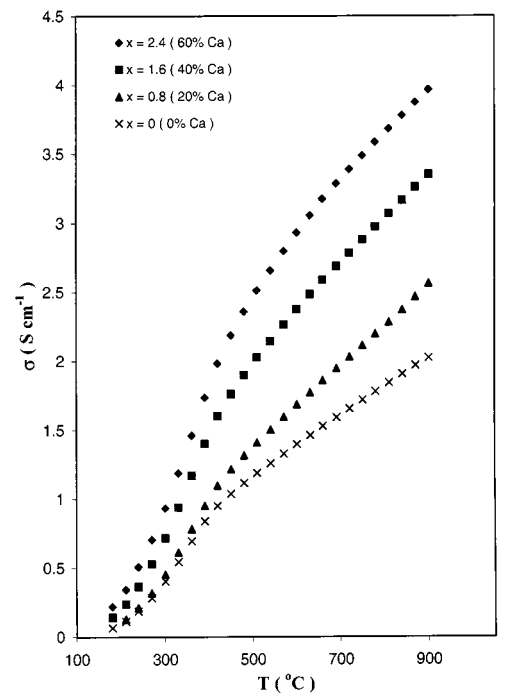

FIG. 8. Variations of total conductivity of $Sr_{4-x}Ca_xFe_{5.4}Co_{0.6}O_{13+\delta}$ (10 atom% Co) with temperature.

(2) The $y = 0$ samples show a change in the slope of the conductivity versus temperature plot around 450°C and such a change in slope vanishes as the Co content increases to 1.5 (Fig. 9). The change in slope becomes more pronounced as the Ca content in the $y = 0$ samples increases, and the samples with $x \ge 1.6$ in Fig. 7 show a decrease in conductivity with increasing temperature at $T > 450$°C. The change in the sign of the slope around 450°C in the $y = 0$ samples at higher Ca contents appears to imply a semiconductor to metal transition (see below).

(3) At a given temperature and Ca content, the conductivity generally increases with increasing Co content, which could be due to an increase in the covalence of the (Fe, Co)–O bonds compared to the Fe–O bonds.

To understand the differences between the $Sr_{4-x}Ca_xFe_6O_{13+\delta}$ and $Sr_{1-x}Ca_xFeO_{3-\delta}$ systems, we synthesized the $Sr_{1-x}Ca_xFeO_{3-\delta}$ samples and measured their conductivity. While the samples with $x \le 0.2$ have the perovskite structure, those with $x \ge 0.4$ have the orthorhombic brownmillerite structure due to a decreasing oxygen content with increasing Ca content. Figure 10 shows the variation of conductivity with temperature for the $Sr_{1-x}Ca_xFeO_{3-\delta}$ system. At a given temperature, the conductivity decreases with

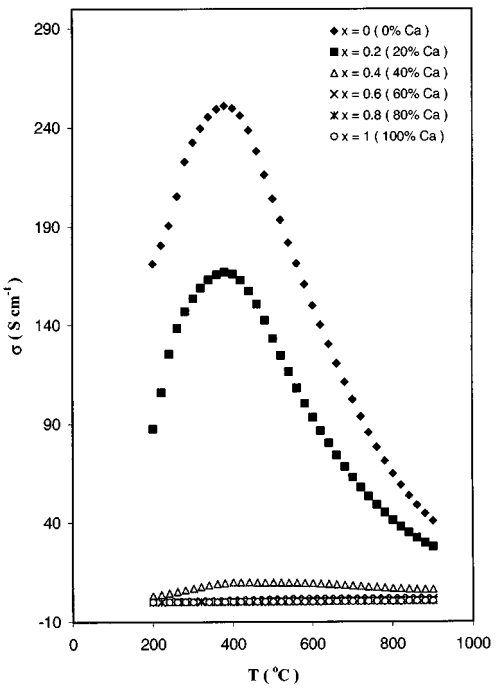

FIG. 10. Variations of total conductivity of $Sr_{1-x}Ca_xFeO_{3-\delta}$ with temperature.

increasing Ca content in $Sr_{1-x}Ca_xFeO_{3-\delta}$, which can be explained as follows: A decreasing oxygen content with increasing Ca content in $Sr_{1-x}Ca_xFeO_{3-\delta}$ will (i) perturb the periodic potential of the Fe–O array and introduce Anderson localized states at the edges of the band and (ii) cause a stronger trapping of the charge carriers. In addition, the substitution of a smaller and less ionic Ca^{2+} for the larger and more ionic Sr^{2+} will cause a decrease in (i) the Fe–O bond angles due to a decreasing tolerance factor t and (ii) the covalence of the Fe–O bonds through inductive effect, both of which will in turn cause a decrease in the bandwidth W. All these factors together cause a decrease in conductivity with increasing Ca content in $Sr_{1-x}Ca_xFeO_{3-\delta}$, despite a decreasing lattice parameter and Fe–O bond length. By contrast, the decrease in lattice parameter and Fe–O bond length with increasing Ca content seems to play a dominant role in $Sr_{4-x}Ca_xFe_6O_{13+\delta}$ to increase the conductivity, despite a small decrease in oxygen content at higher Ca contents (Fig. 5). A decreasing Fe–O bond length tends to increase the Fe–O interaction and the conductivity.

To understand the origin of the change in the sign of the slope of the conductivity versus temperature plots around 450°C in $Sr_{4-x}Ca_xFe_6O_{13+\delta}$ for $x \geq 1.6$ (Fig. 7) and around 350°C in $Sr_{1-x}Ca_xFeO_{3-\delta}$ for $x \leq 0.2$ (Fig. 10), we recorded the TGA plots both in N_2 atm and in a mixture of 70% N_2 and 30% O_2. The TGA plots of $Sr_{1.2}Ca_{2.8}Fe_6O_{13+\delta}$ (70 atom% Ca) and $SrFeO_{3-\delta}$ are shown, respectively, in

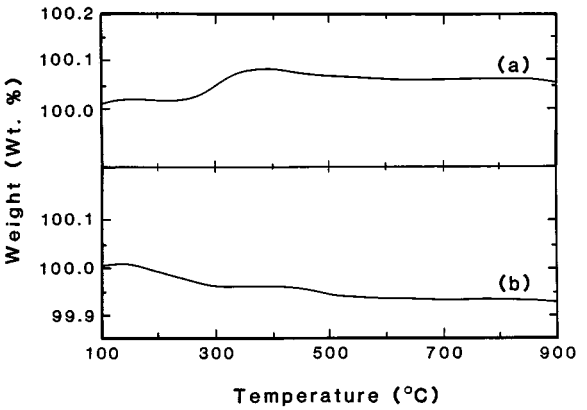

FIG. 11. TGA plots of $Sr_{1.2}Ca_{2.8}Fe_6O_{13+\delta}$ recorded in (a) a mixture of 70% N_2 and 30% O_2 and (b) N_2 atm with a heating rate of 2°C/min.

Figs. 11 and 12. The slight increase in oxygen content around 300°C in both Figs. 11a and 12a is due to an atmosphere slightly richer in oxygen (70% N_2–30% O_2) as used in the TGA experiments compared to the ambient air. A comparison of the data in Figs. 11 and 12 reveals that, while the perovskite phase $SrFeO_{3-\delta}$ loses a significant amount of oxygen above 350°C, $Sr_{1.2}Ca_{2.8}Fe_6O_{13+\delta}$ is remarkably stable up to about 900°C.

The TGA data suggests that the change in the sign of the slope around 350°C and the decrease in conductivity with increasing temperature for $T > 350$°C in $SrCa_xFeO_{3-\delta}$ for $x \leq 0.2$ (Fig. 10) is due to the oxygen loss. The increasing concentration of oxygen vacancies at $T > 350$°C results in an increasing trapping of carriers and a decrease in

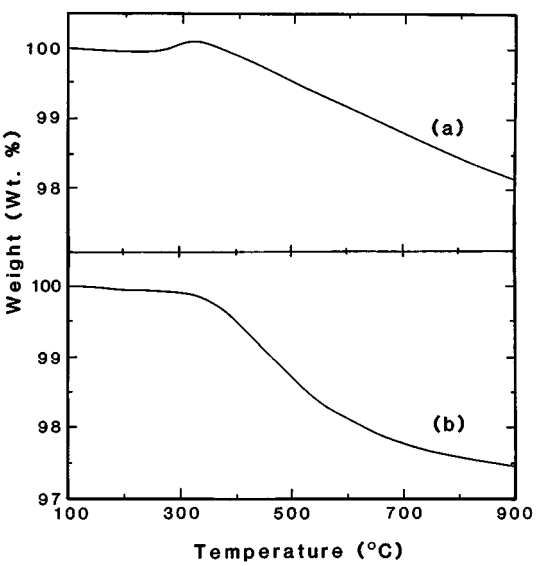

FIG. 12. TGA plots of $SrFeO_{3-\delta}$ recorded in (a) a mixture of 70% N_2 and 30% O_2 and (b) N_2 atm with a heating rate of 2°C/min.

conductivity. A similar observation (19, 20) in the system $La_{1-x}Sr_xFe_{0.8}Co_{0.2}O_{3-\delta}$ has also been previously attributed to oxygen loss (20). On the other hand, the absence of any oxygen loss in the system $Sr_{4-x}Ca_xFe_6O_{13+\delta}$ (Fig. 11) suggests that the change in the sign of the slope around 450°C and the decrease in conductivity with increasing temperature for $T > 450$°C (Fig. 7) for $x \geq 1.6$ is not linked to changes in oxygen stoichiometry.

To understand the origin of this transition, we have carried out both X-ray diffraction and thermoelectric power measurements as a function of temperature. No detectable change was observed in the X-ray diffraction patterns of, for example, $Sr_{1.2}Ca_{2.8}Fe_6O_{13+\delta}$, at least up to 750°C, indicating that the observed transition in the conductivity is not due to any macroscopic structural change. The variations of thermoeletric power α with temperature are shown in Fig. 13 for various x values in $Sr_{4-x}Ca_xFe_6O_{13+\delta}$. The thermoelectric power is positive for all the three samples, indicating that holes are the majority carriers. The absolute values of the thermoelectric power are high, indicating typical semiconductor behavior. The thermoelectric power at a given temperature decreases with increasing Ca content, which is consistent with the increasing conductivity. While the value of α decreases with increasing temperature for $T < 450$°C (semiconducting behavior) for all values of x, it remains almost constant for $x = 0$ and begins to increase for $x \geq 1.6$ with increasing temperature for $T > 450$°C. Thus, the change in temperature variation of α around 450°C is consistent with the changes in the temperature variation of conductivity around 450°C (Fig. 7). Although the increase in α and the decrease in conductivity with temperature for $T > 450$°C in the samples with $x \geq 1.6$ may be similar to those expected for metallic behavior, the absolute value of α is much larger than that expected for metallic samples.

The high value of thermoelectric power and an average oxidation state $< 3.2+$ for Fe suggest that the $Sr_{4-x}Ca_xFe_6O_{13+\delta}$ ($x \geq 1.6$) samples are not metallic at $T > 450$°C. One possible reason for the observed transition in the conductivity behavior around 450°C could be a beginning of a redistribution of charge carriers between the perovskite FeO_2 and the nonperovskite $Fe_2O_{2.5}$ layers. An examination of the net charge distribution along the b axis of the $Sr_4Fe_6O_{13}$ structure in Fig. 1, assuming an oxygen content of 13 and all Fe^{3+}, reveals a net charge of -1 in the perovskite layer and $+1$ in the nonperovskite layer. It is quite possible that the Fe atoms in the two layers may have slightly different oxidation states. For example, a net negative charge in the FeO_2 layer and a net positive charge in the $Fe_2O_{2.5}$ layer as indicated in Fig. 1 may lead to an actual Fe oxidation state higher than $3+$ in the FeO_2 layer and lower than $3+$ in the $Fe_2O_{2.5}$ layer.

It is possible that at $T > 450$°C, a transfer of electrons from the $Fe_2O_{2.5}$ layer to the FeO_2 layer may begin to occur to lower the oxidation state of Fe in the FeO_2 layer.

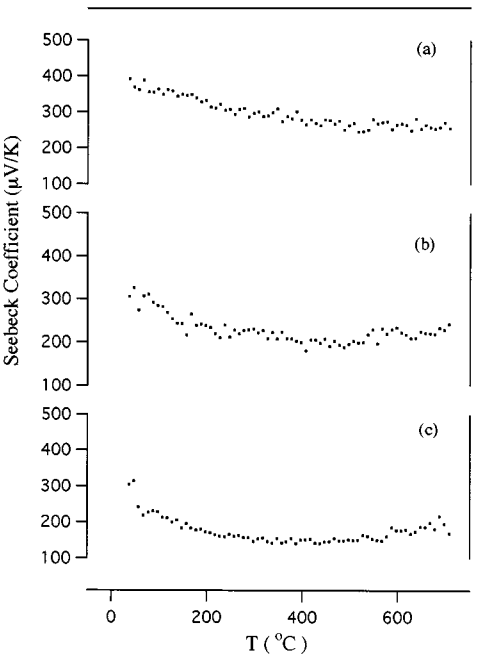

FIG. 13. Variations of thermoelectric power of $Sr_{4-x}Ca_xFe_6O_{13+\delta}$ with temperature: (a) $x = 0$, (b) $x = 1.6$, and (c) $x = 2.8$.

Such a transfer will in turn result in a decrease in the hole concentration and conductivity in the FeO_2 layer with increasing temperature. If the perovskite layer is more conductive than the nonperovskite layer, this will result in a decrease in the total conductivity with increasing temperature. The redistribution of charges between the two types of layers may be facilitated by, for example, changes in bond lengths arising from thermal expansion mismatches. The substitution of a smaller and less ionic Ca^{2+} for Sr^{2+} may very well enhance such charge redistribution and cause a decrease in conductivity with temperature at $T > 450$°C.

Finally, we have investigated the effect of other transition metal ions on the observed transition in conductivity by replacing Fe with 2 atom% Mn, Co, Ni, and Cu. The variations of conductivity with temperature are shown in Fig. 14 for $Sr_{1.2}Ca_{2.8}Fe_{5.88}M_{0.12}O_{13+\delta}$ (M = Mn, Co, Ni, and Cu). The effect of Mn substitution even at a level of 2 atom% is so drastic that it completely eliminates the change in the slope of the conductivity versus temperature plot. It also decreases the conductivity significantly. On the other hand, the substitutions of 2 atom% Co, Ni, and Cu for Fe not only shift the temperature at which the slope changes to higher temperatures but also eliminates the negative slope at higher temperatures in the conductivity versus temperature plot. These results suggest that, whatever may be the origin of the transition in the conductivity behavior, the transition is very sensitive to the substitution of trace amounts of other transition metal ions.

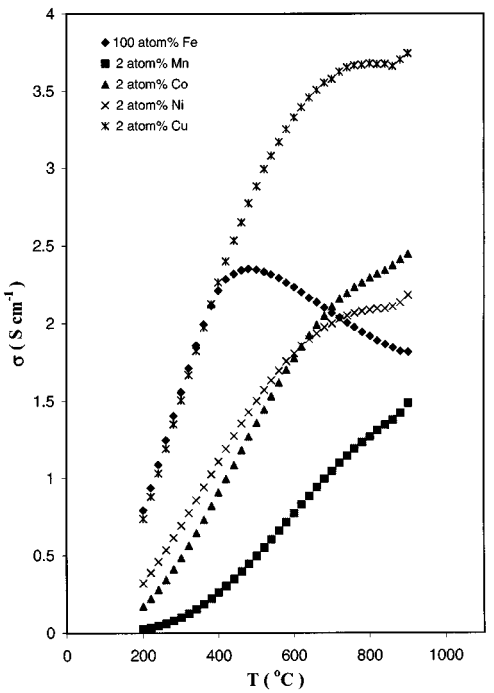

FIG. 14. Variations of total conductivity of $Sr_{1.2}Ca_{2.8}Fe_{5.88}M_{0.12}O_{13+\delta}$ (M = Mn, Co, Ni, and Cu) with temperature.

4. CONCLUSIONS

The crystal chemistry and electrical properties of $Sr_{4-x}Ca_xFe_{6-y}Co_yO_{13+\delta}$ having a perovskite-related intergrowth structure have been investigated. The cell parameters, cell volume, oxygen content, and oxidation state decrease with increasing Ca content x. The $Sr_{4-x}Ca_xFe_6O_{13+\delta}$ samples with $x \geq 1.6$ exhibit an interesting transition from positive to negative temperature variation of conductivity at around 450°C. In the absence of any noticeable oxygen loss or structrual changes and with a high value of thermoelectric power, the transition is attributed to a possible redistribution of charge carriers between the perovskite and nonperovskite layers. The transition is found to be sensitive to trace amounts of doping with other transition metals such as Mn, Co, Ni, and Cu. The oxygen permeation studies of the $Sr_{4-x}Ca_xFe_{6-y}Co_yO_{13+\delta}$ systems are currently in progress in our laboratory.

ACKNOWLEDGMENTS

Acknowledgement is made to the donors of The Petroleum Research Fund, administered by the ACS (Grant ACS-PRF # 32410-AC5), and the Welch Foundation (Grant F-1254) for support of this research.

REFERENCES

1. J. G. Bednorz and K. A. Muller, *Z. Phys. B* **64,** 189 (1986).
2. R. Von Helmolt, J. Wecker, B. Holzapfelh, L. Schultz, and K. Samwer, *Phys. Rev. Lett.* **71,** 2331 (1993).
3. T. Ishihara, H. Matruda, and Y. Takita, *J. Amer. Chem. Soc.* **116,** 3801 (1994).
4. I. Riess, *in* "The CRC Handbook of Solid State Electrochemistry" (P. J. Gellings and H. J. M. Bouwmeester, Eds.), p. 223. CRC Press, New York, 1997.
5. Y. Teraoka, H. Zhang, S. Furukawa, and N. Yamazoe, *Chem. Lett.* 1743 (1985).
6. Y. Teraoka, H. Zhang, K. Okamoto, and N. Yamazoe, *Mater. Res. Bull.* **23,** 51 (1988).
7. H. Kruidhof, H. J. M. Bouwmeester, R. H. E. v. Doorn, and A. J. Burggaraaaf, *Solid State Inoics* **63/65,** 816 (1993).
8. L. Qui, T. H. Lee, L.-M. Liu, Y. L. Yang, and A. J. Jacobson, *Solid State Ionics* **76,** 321 (1995).
9. H. U. Anderson, *Solid State Ionics* **52,** 33 (1992).
10. B. Ma, J.-H. Park, C. U. Segre, and U. Balachandran, *Mater. Res. Soc. Symp. Proc.* **393,** 49 (1995).
11. B. Ma, U. Balachandran, J.-H. Park, and C. U. Segre, *Solid State Ionics* **83,** 65 (1996).
12. B. Ma, U. Balachandran, and J.-H. Park, *J. Electrochem. Soc.* **143,** 1736 (1996).
13. S. Guggilla and A. Manthiram, *J. Electrochem. Soc.* **144,** L120 (1997).
14. A. Yoshiasa, K. Ueno, F. Kanamaru, and H. Horiuchi, *Mater. Res. Bull.* **21,** 175 (1986).
15. F. Kanamaru, S. Shimada, and M. Koizumi, *J. Phys. Chem. Solids* **33,** 1169 (1972).
16. S. Kim, Y. L. Yang, R. Christoffersen, and A. J. Jacobson, *Mater. Res. Soc. Symp. Proc.* **496,** 249 (1998).
17. T. Armstrong, S. Guggilla, and A. Manthiram, *Mater. Res. Bull.*, in press.
18. A. Manthiram, S. Swinnea, Z. T. Sui, H. Steinfink, and J. B. Goodenough, *J. Amer. Chem. Soc.* **109,** 6667 (1987).
19. L.-W. Tai, M. M. Nasrallah, H. U. Anderson, D. M. Sparlin, and S. R. Sehlin, *Solid State Ionics* **76,** 259 (1995).
20. L.-W. Tai, M. M. Nasrallah, H. U. Anderson, D. M. Sparlin, and S. R. Sehlin, *Solid State Ionics* **76,** 273 (1995).